

Embodied Language Grounding with Implicit 3D Visual Feature Representations

Mihir Prabhudesai*, Hsiao-Yu Fish Tung*, Syed Ashar Javed *

Maximilian Sieb†, Adam W. Harley, Katerina Fragkiadaki

{mprabhud, htung, sajaved, aharley, msieb, katef}@cs.cmu.edu

Carnegie Mellon University

Abstract

The hypothesis of simulation semantics suggests that people think and reason about language utterances visually. It formally states that processing words and sentences leads to perceptual and motor simulations of explicitly and implicitly mentioned aspects of linguistic content. This work proposes a computational model of simulation semantics that associates language utterances to 3D visual abstractions of the scene they describe. The 3D visual abstractions are encoded as a 3-dimensional visual feature maps. We infer such 3D visual scene feature maps from RGB images of the scene via view prediction: the generated 3D scene feature map when neurally projected from a camera viewpoint it should match the corresponding RGB image. The models we propose have two functionalities: i) conditioned on the dependency tree of an utterance, they generate the related visual 3D feature map and reason about its plausibility (without access to any visual input), and ii) conditioned on the dependency tree of a referential expression and a related image they localize object referents in the 3D feature map inferred from the image. We empirically show our model outperforms by a large margin models of language and vision that associate language with 2D CNN activations or 2D images in a variety of tasks, such as, classifying plausibility of utterances by spatially reasoning over possible and impossible object configurations, 3D object referential detection, inferring desired scene transformations given language instructions, and providing rewards for trajectory optimization of corresponding policies. We attribute the improved performance of our model to its improved generalization across camera viewpoints and reasoning of possible object arrangements, benefits of its 3D visual grounding space, in place of view-dependent images and CNN image features.

1. Introduction

Consider the utterance “the tomato is to the left of the pot”. Humans can answer numerous questions about the situation described, as well as reason through alternatives, such as, “is the pot larger than the tomato?”, “can we move to a viewpoint from which the tomato is completely hidden behind the pot?”, “can we have an object that is both to the left of the tomato and to the right of the pot?”, and so on. How can we learn computational models that would permit a machine to carry out similar types of reasoning that humans are capable of? One possibility is to treat the task as text comprehension [Weston et al. \(2014\)](#); [Hermann et al. \(2015\)](#); [Kadlec et al. \(2016\)](#); [Dhingra et al. \(2016\)](#) and train machine learning models using supervision from utterances accompanied with question / answer pairs. However, information needed for answering the questions is not contained in the utterance itself; training a model to carry out predictions in absence of the relevant information would lead to overfitting. Associating utterances with RGB images that depict the scene described in the utterance, and using both images and utterances for answering questions provides more world context and has been shown to be helpful. Consider though that information about object size, object extent, occlusion relationships, free space and so on, are only indirectly present in an RGB image, while they are readily available given a 3D representation of the scene the image depicts. Though it would take many training examples to learn whether a spoon can be placed in between the tomato and the pot on the table, in 3D such experiment can be mentally carried out easily, simply by considering whether the 3D model of the spoon can fit in the free space between the tomato and the pot. Humans are experts in inverting camera projection and inferring an approximate 3D scene given an RGB image [Olshausen \(2013\)](#). This paper similarly builds upon inverse graphics neural architectures for providing the 3D visual representations to associate language, with the hope to inject spatial reasoning capabilities into architectures for language understanding.

*Equal contribution

†Work done while in Carnegie Mellon University.

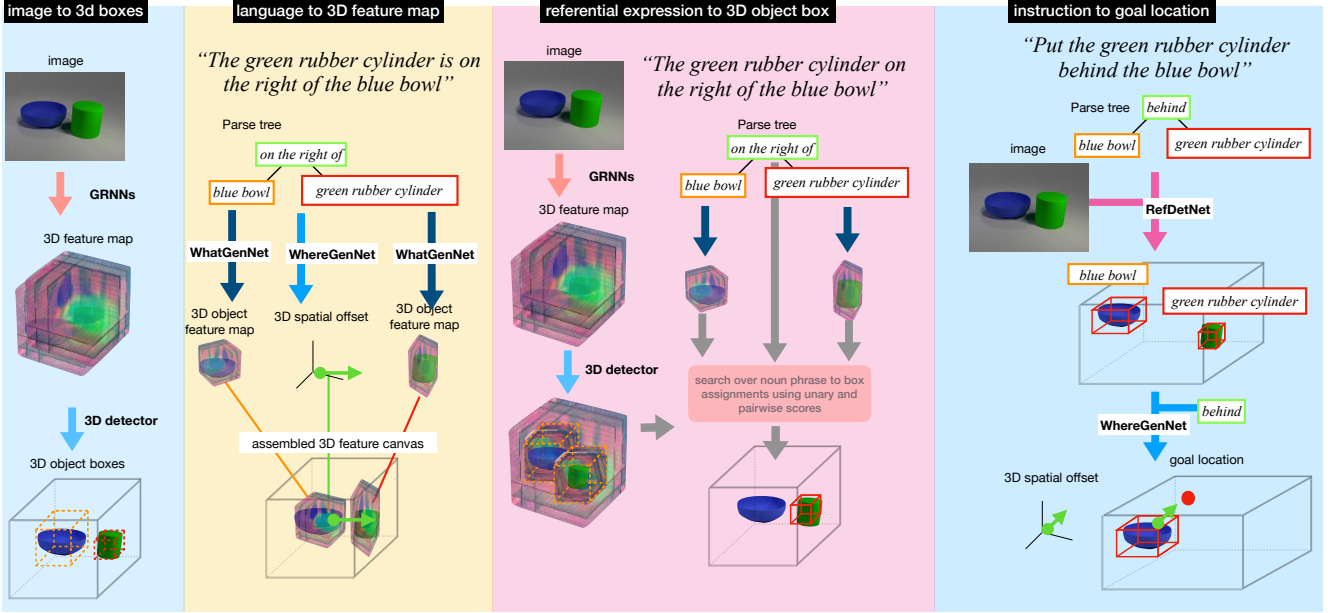


Figure 1: **Embodied language grounding with implicit 3D visual feature representations.** Our model associates utterances with 3D scene feature representations. We map RGB images to 3D scene feature representations and 3D object boxes of the objects present building upon the method of Tung et al. [Tung et al. \(2019\)](#) (column 1). We map an utterance and its dependency tree to object-centric 3D feature maps and cross-object relative 3D offsets using stochastic generative networks (column 2). We map a referential expression to the 3D box of the object referent (column 3). Last, given a placement instruction, we 3D localize the referents in the scene and infer the 3D desired location for the object to be manipulated (column 4). We use predicted location to supply rewards for trajectory optimization of placement policies.

We propose associating language utterances to space-aware 3D visual feature representations of the scene they describe. We infer such 3D scene representations from RGB images of the scene. Though inferring 3D scene representations from RGB images, a.k.a. inverse graphics is known to be a difficult problem [Kulkarni et al. \(2015\)](#); [Romaszko et al. \(2017\)](#); [Tung et al. \(2017\)](#), we build upon recent advances in computer vision [Tung et al. \(2019\)](#) that consider inferring from images a learnable 3D scene feature representation in place of explicit 3D representations such as meshes, pointclouds or binary voxel occupancies pursued in previous inverse graphics research [Kulkarni et al. \(2015\)](#); [Romaszko et al. \(2017\)](#); [Tung et al. \(2017\)](#). Such learnable 3D scene feature map emerges in a self-supervised manner by optimizing for view prediction in neural architectures with geometry-aware 3D representation bottlenecks, as described in previous work of Tung et al. [Tung et al. \(2019\)](#). After training, these architectures learn to map RGB video streams or single RGB images to complete 3D feature maps of the scene they depict, inpainting by imagination occluded or missing details of the 2D image input. **The contribution of our work is to use such 3D feature representations for language understanding and spatial reasoning.** We train

modular generative networks that condition on the dependency tree of the utterance and predict a 3D feature map of the scene the utterance describes. They do so by predicting appearance and relative 3D location of objects, and updating a 3D feature workspace, as shown in Figure 1, 2nd column. We further train modular discriminative networks that condition on a referential expression and detect the object referred to in the 3D feature map of the input RGB image, by scoring object appearances and cross-object spatial arrangements, respectively, as shown in Figure 1, 3rd column. We call our model *embodied* since training the 2D image to 3D feature mapping requires supervision from a mobile—or more generally embodied—agent that moves around in the 3D world, collects (posed) images and learns to predict visual results of its motion.

We demonstrate the benefits of associating language to 3D visual feature scene representations in three basic language understanding tasks:

(1) Affordability reasoning Our model can classify affordable (plausible) and unaffordable (implausible) spatial expressions. For example, “A to the left of B, B to the left of C, C to the right of A” describes a plausible configuration, while “A to the left of B, B to the left of C, C to the left of A”

describes a non-plausible scene configuration, where A, B, C any object mentions. Our model reasons about plausibility of object arrangements in the inferred 3D feature map, where free space and object 3D intersection can easily be learnt/evaluated, as opposed to 2D image space.

(2) Referential expression detection Given a referential spatial expression, e.g., “*the blue sphere behind the yellow cube*”, and an RGB image, our model outputs the 3D object bounding box of the referent in the inferred 3D feature map, as shown in Figure 1 3rd column. Our 3D referential detector generalizes across camera viewpoints better than existing state-of-the-art 2D referential detectors Hu et al. (2016) thanks to the view invariant 3D feature representation.

(3) Instruction following Given an object placement instruction, e.g., “*put the cube behind the book*”, our referential 3D object detector identifies the object to be manipulated and our generative network predicts its desired 3D goal location, as shown in Figure 1 4th column. We use such 3D goal location in trajectory optimization of object placement policies. We show our model successfully executes natural language instructions.

In each task we compare against existing state-of-the-art models: the language-to-2D image generation model of Deng et al. (2018) and the 2D referential object detector of Hu et al. (2016), which we adapt to have same input as our model. Our model outperforms the baselines by a large margin in each of the three tasks. We further show strong generalization of natural language learnt concepts from the simulation to the real world thanks to the what-where decomposition employed in our generative and detection networks, where spatial expression detectors only use 3D spatial information, as opposed to object appearance and generalize to drastically different looking scenes without any further annotations. Our model’s improved performance is attributed to i) its improved generalization across camera placements thanks to the viewpoint invariant 3D feature representations, ii) its improved performance on free-space inference and plausible object placement in 3D over 2D. Many physical properties can be trivially evaluated in 3D while they need to be learned by a large number of training examples in 2D with questionable generalization across camera viewpoints. 3D object intersection is one such important property, very useful for spatial reasoning of plausible object arrangements. Our datasets and code will be made publicly available upon publication to facilitate reproducibility of our work.

2. Related Work

Learning and representing common sense world knowledge for language understanding is a major open research question. Researchers have considered grounding natural language on visual cues as a means of injecting visual common sense to natural language understanding Rohrbach

et al. (2013); Fang et al. (2015); Rohrbach et al. (2013); Fang et al. (2015); Antol et al. (2015); Devlin et al. (2015); Andreas et al. (2016); Rohrbach et al. (2012, 2017, 2015); Karpathy and Fei-Fei (2015); Yang et al. (2015); Donahue et al. (2015); Deng et al. (2018). For example visual question answering is a task that has attracted a lot of attention and whose performance has been steadily improving over the years Shah et al. (2019). Yet, there is vast knowledge regarding basic physics and mechanics that current vision and language models miss, as explained in Vedantam et al. (2015). For example, existing models cannot infer whether “*the mug inside the pen*” or “*the pen inside the mug*” is more plausible, whether “*A in front of B, B in front of C, C in front of A*” is realisable, whether the mug continues to exist if the camera changes viewpoint, and so on. It is further unclear what supervision is necessary for such reasoning ability to emerge in current model architectures.

3. Language grounding on 3D visual feature representations

We consider a dataset of 3D static scenes annotated with corresponding language descriptions and their dependency trees, as well as a reference camera viewpoint. We further assume access at training time to 3D object bounding boxes and correspondences between 3D object boxes and noun phrases in the language dependency trees. The language utterances we use describe object spatial arrangements and are programmatically generated, same as their dependency trees, using the method described in Johnson et al. (2016). We infer 3D feature maps of the world scenes from RGB images using Geometry-aware Recurrent Neural Nets (GRNNs) of Tung et al. Tung et al. (2019), which we describe for completeness in Section 3.1. GRNNs learn to map 2D image streams to 3D visual feature maps while optimizing for view prediction, without any language supervision. In Section 3.2, we describe our proposed generative networks that condition on the dependency tree of a language utterance and generate an object-factorized 3D feature map of the scene the utterance depicts. In Section 3.3, we describe discriminative networks that condition on the dependency tree of a language utterance and the inferred 3D feature map from the RGB image and localize in 3D the object being referred to. In Section 3.4, we show how our generative and discriminative networks of Sections 3.2, 3.3 can be used for following object placement instructions.

3.1. Inverse graphics with Geometry-aware Recurrent Neural Nets (GRNNs)

GRNNs learn to map an RGB or RGB-D (RGB and depth) image or image sequence that depicts a static 3D world scene to a 3D feature map of the scene in an end-to-end differentiable manner while optimizing for view prediction: the inferred 3D feature maps, when projected

from designated camera viewpoints, are neurally decoded to 2D RGB images and the weights of the neural architecture are trained to minimize RGB distance of the predicted image from the corresponding ground-truth RGB image view. We will denote the inferred 3D feature map as $\mathbf{M} \in \mathbb{R}^{W \times H \times D \times C}$ —where W, H, D, C stand for width, height, depth and number of feature channels, respectively. Every (x, y, z) grid location in the 3D feature map \mathbf{M} holds 1-dimensional feature vector that describes the semantic and geometric properties of a corresponding 3D physical location in the 3D world scene. The map is updated with each new video frame while estimating and cancelling camera motion, so that information from 2D pixels that correspond to the same 3D physical point end-up nearby in the map. At training time, we assume a mobile agent that moves around in a 3D world scene and sees it from multiple camera viewpoints, in order to provide “labels” for view prediction to GRNNs. Upon training, GRNNs can map an RGB or RGB-D image sequence or single image to a complete 3D feature map of the scene it depicts, i.e., it learns to *imagine* the missing or occluded information; we denote this 2D-to-3D mapping as $\mathbf{M} = \text{GRNN}(I)$ for an input RGB image I .

3D object proposals. Given images with annotated 3D object boxes, work of Tung et al. [Tung et al. \(2019\)](#) trained GRNNs for 3D object detection by learning a neural module that takes as input the 3D feature map \mathbf{M} inferred from the input image and outputs 3D bounding boxes and binary 3D voxel occupancies (3D segmentations) for the objects present in the map. Their work essentially adapted the state-of-the-art 2D object detector Mask-RCNN [He et al. \(2017\)](#) to have 3D input and output instead of 2D. We use the same architecture for our category-agnostic 3D region proposal network (3D RPN) in Section 3.3. For further details on GRNNs, please read [Tung et al. \(2019\)](#).

3.2. Language-conditioned 3D visual imagination

We train generative networks to map language utterances to 3D feature maps of the scene they describe. They do so using a compositional generation process that conditions on the dependency tree of the utterance (assumed given) and generates one object at a time, predicting its appearance and location using two separate stochastic neural modules, *what* and *where*, as shown in Figure 2.

The *what* generation module $G_A(p, z; \phi)$ is a stochastic generative network of object-centric appearance that given a noun phrase p learns to map the word embeddings of each adjective and noun and a random vector of sampled Gaussian noise $z \in \mathbb{R}^{50} \sim \mathcal{N}(0, I)$ to a corresponding fixed size 3D feature tensor $\hat{\mathbf{M}}^o \in \mathbb{R}^{w \times h \times d \times c}$ and a size vector $s^o \in \mathbb{R}^3$ that describes the width, height, and depth for the tensor. We resize the 3D feature tensor $\hat{\mathbf{M}}^o$ to have the predicted size s^o and obtain $\mathbf{M}^o = \text{Resize}(\hat{\mathbf{M}}^o, s^o)$. We use a gated mixture of experts [Shazeer et al. \(2017\)](#) layer—

a gated version of point-wise multiplication—to aggregate outputs from different adjectives and nouns, as shown in Figure 2.

The *where* generation module $G_S(s, z, \psi)$ is a stochastic generative network of cross-object 3D offsets that learns to map the one-hot encoding of a spatial expression s , e.g., “in front of”, and a random vector of sampled Gaussian noise $z \in \mathbb{R}^{50} \sim \mathcal{N}(0, I)$ to a relative 3D spatial offset $d\mathbf{X}^{(i,j)} = (dX, dY, dZ) \in \mathbb{R}^3$ between the corresponding objects. Let b_i^o denote the 3D spatial coordinates of the corners of a generated object.

Our complete generative network conditions on the dependency parse tree of the utterance and adds one 3D object tensor $\mathbf{M}_i^o, i = 1 \dots K$ at a time to a 3-dimensional feature canvas according to their predicted 3D locations, where K is the number of noun phrases in the dependency tree: $\mathbf{M}^g = \sum_{i=1}^K \text{DRAW}(\mathbf{M}_i^o, \mathbf{X}_i^o)$, where DRAW denotes the operation of adding a 3D feature tensor to a 3D location. The 3D location \mathbf{X}^1 of the first object is chosen arbitrarily, and the locations of the rest of the object is based the predicted cross-object offsets: $\mathbf{X}_2^o = \mathbf{X}_1^o + d\mathbf{X}^{(2,1)}$. If two added objects intersect in 3D, i.e., the intersection over union of the 3D object bounding boxes is above a cross-validated threshold of 0.1, $\text{IoU}(b_i^o, b_j^o) > 0.1$, we re-sample object locations until we find a scene configuration where objects do not 3D intersect, or until we reach a maximum number of samples—in which case we infer the utterance is impossible to realize. By exploiting the constraint of non 3D intersection in the 3D feature space, our model can both generalize to longer parse trees than those seen at training time—by re-sampling until all spatial constraints are satisfied—as well as infer plausibility of utterances, as we validate empirically in Section 4.2. In 3D, non-physically plausible object intersection is easy to delineate from physically plausible object occlusion, something that is not easy to infer with 2D object coordinates, as we show empirically in Section 4.2, or at least you would need a much much larger number of *annotated* training examples to do so. Given the 3D coordinates of two 3D bounding boxes 3D intersection over union is easy to learn with a classifier, but we simply use thresholding of the computed 3D intersection over union.

We train our stochastic generative networks using conditional variational autoencoders. We detail the corresponding inference networks in Section 1 of the supplementary file due to lack of space.

3.3. Detecting referential expressions in 3D

We train discriminative networks to map spatial referential expressions, e.g., “the blue cube to the right of the yellow sphere behind the green cylinder” and related RGB images, to the 3D bounding box of the objects the expressions refer to. They do so using a compositional detection process

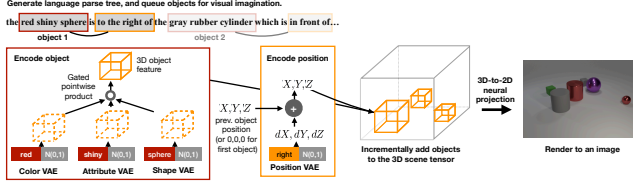


Figure 2: **Mapping language utterances to object-centric appearance tensors and cross-object 3D spatial offsets** using conditional *what-where* generative networks.

that conditions on the dependency tree of the referential expression (assumed given) and predicts a 3D appearance detector template for each noun phrase, used to compute an object appearance score, and 3D spatial classifier for each spatial expression, used to compute a spatial compatibility score, as we detail below. Such compositional structure of our detector is necessary to handle referential expressions of arbitrary length. Our detector is comprised of a *what* detection module and a *where* detection module, as shown in Figure 3. The *what* module $D_A(p; \xi)$ is a neural network that given a noun phrase p learns to map the word embeddings of each adjective and noun to a corresponding fixed-size 3D feature tensor $f = D_A(p; \xi) \in \mathbb{R}^{w \times h \times d \times c}$, we used $w = h = d = 16$ and $c = 32$. Our *what* detection module is essentially a deterministic alternative of the *what* generative stochastic network of Section 3.2. The object appearance score is obtained by computing inner-product between the detection template $D_A(p; \xi)$ and the cropped object 3D feature map $\text{CropAndResize}(\mathbf{M}, b^o)$, where $\mathbf{M} = \text{GRNN}(I)$ and b^o the 3D box of the object. We feed the output of the inner product to a sigmoid activation layer.

The *where* detection module $D_S(s, b_1^o, b_2^o; \omega)$ takes as input the 3D box coordinates of the hypothesized pair of objects under consideration, and the one-hot encoding of the spatial utterance s (e.g., “in front of”, “behind”), and predicts a score whether the two-object configuration matches the spatial expression.

We train both the *what* and *where* detection modules in a supervised way. During training, we use ground-truth associations of noun phrases p to 3D object boxes in the image for positive examples, and random crops or other objects as negative examples. For cropping, we use ground-truth 3D object boxes at training time and detected 3D object box proposals from the 3D region proposal network (RPN) of Section 3.1 at test time. We use positive examples from our training set and negative examples from competing expressions as well as synthetic 3D object boxes in random locations.

Having trained our *what* and *where* detector modules, and given the dependency parse tree of an utterance and a set of bottom up 3D object proposals, we exhaustively search over assignments of noun phrases to detected 3D ob-

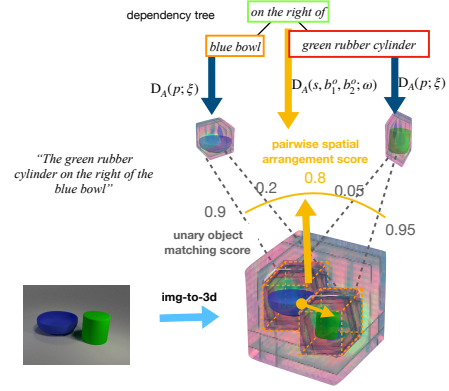


Figure 3: **3D referential object detection.** We exhaustively score all possible assignments of noun phrases to detected 3D bounding boxes. Each assignment is scored based on unary appearance scores and pairwise spatial scores, as described in the text.

jects in the scene. We only keep noun phrase to 3D box assignments if their unary matching score is above a cross-validated threshold of 0.4. Then, we simply pick the assignment of noun phrases to 3D boxes with the highest product of unary and pairwise scores. Our 3D referential detector resembles previous 2D referential detectors Hu et al. (2016); Cirik et al. (2018), but operates in 3D appearance features and spatial arrangements, instead of 2D.

3.4. Instruction following

Humans use natural language to program fellow humans e.g., “please, put the orange inside the wooden bowl”. We would like to be able to program robotic agents in a similar manner. Most current policy learning methods use manually coded reward functions in simulation or instrumented environments to train policies, as opposed to visual detectors of natural language expressions Tung and Fragkiadaki (2018). If visual detectors of “orange inside the wooden basket” were available, we would use them to automatically monitor an agent’s progress towards achieving the desired goal and supply rewards accordingly, as opposed to hard-coding them in the environment.

We use the language-conditioned generative and detection models proposed in Section 3.2, 3.3 to obtain a reliable perceptual reward detector for object placement instructions with the following steps, as shown in Figure 1 4th column: (1) We localize in 3D all objects mentioned in the instruction using the aforementioned 3D referential detectors. (2) We predict the desired 3D goal location for the object to be manipulated \mathbf{x}_{goal}^o using our stochastic spatial arrangement generative network $G_S(s, z; \psi)$. (3) We compute per time step costs being proportional to the Euclidean distance of the current 3D location of the object \mathbf{x}_t^o and end-effector 3D

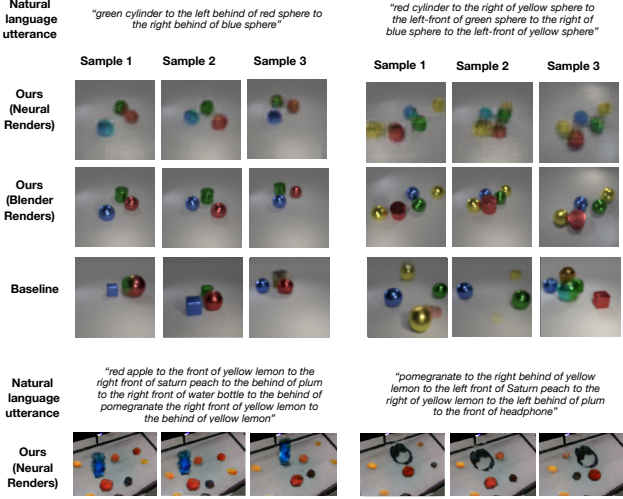


Figure 4: **Language to scene generation** (Rows 1,2,4) and **Language to image generation** (Row 3) from our model and the model of Deng et al [Deng et al. \(2018\)](#) for utterances longer than those encountered at training time. Both our model and the baseline are stochastic, and we sample three generated scenes/images per utterance.

location \mathbf{x}_t^e assumed known from forward dynamics, and the desired 3D goal object location \mathbf{x}_{goal}^o and end-effector 3D location \mathbf{x}_{goal}^e : $\mathcal{C}_t = \|\mathbf{x}_t - \mathbf{x}_{goal}\|_2^2$, where $\mathbf{x}_t = [\mathbf{x}_t^o; \mathbf{x}_t^e]$ is the concatenation of object and end-effector state at time step t and $\mathbf{x}_{goal} = [\mathbf{x}_{goal}^o; \mathbf{x}_{goal}^e]$. We formulate this as a reinforcement learning problem, where at each time step the cost is given by $c_t = \|\mathbf{x}_t - \mathbf{x}_{goal}\|_2$. We use i-LQR (iterative Linear Quadratic Regulator) [Tassa et al. \(2014\)](#) to minimize the cost function $\sum_{t=1}^T \mathcal{C}_t$. I-LQR learns a time-dependent policy $\pi_t(\mathbf{u}|\mathbf{x}; \theta) = \mathcal{N}(\mathbf{K}_t \mathbf{x}_t + \mathbf{k}_t, \Sigma_t)$, where the time-dependent control gains are learned by model-based updates, where the dynamical model $p(\mathbf{x}_t | \mathbf{x}_{t-1}, \mathbf{u}_t)$ of the *a priori* unknown dynamics is learned during training time. The actions \mathbf{u} are defined as the changes in the robot end-effector’s 3D position and orientation about the vertical axis, giving a 4-dimensional action space.

We show in Section 4.4 that our method successfully trains multiple language-conditioned policies. In comparison, 2D desired goal locations generated by 2D baselines [Tung and Fragkiadaki \(2018\)](#) often fail to do so.

4. Experiments

We test the proposed language grounding model in the following tasks: (i) Generating scenes based on language utterances (ii) classifying utterances based on whether they describe possible or impossible scenes, (iii) detecting spatial referential expressions, and, (iv) following object placement instructions. We consider two datasets: (i) The

CLEVR dataset of Johnson et al. [Johnson et al. \(2016\)](#) that contains 3D scenes annotated with natural language descriptions, their dependency parse trees, and the object 3D bounding boxes. The dataset contains Blender generated 3D scenes with geometric objects (Figure 1). Each object can take a number of colors, materials, shapes and sizes. Each scene is accompanied with a description of the object spatial arrangements, as well as its parse tree. Each scene is rendered from 12 azimuths and 4 elevation angles, namely, $\{20^\circ, 40^\circ, 60^\circ, 12^\circ\}$. We train GRNNs for view prediction using the RGB image views in the training sets. The annotated 3D bounding boxes are used to train our 3D object detector. We generate 800 scenes for training, and 400 for testing. The language is generated randomly with a restriction to have **maximum 2 objects** for the training scenes. (ii) A veggie arrangement dataset we collected in the real world. We built a camera dome comprised of 8 cameras placed in a hemisphere above a table surface. We move vegetables around and collect multiview images. We automatically annotate the scene with 3D object boxes by doing 3D point-cloud subtraction at training time, we use the obtained 3D boxes to train our 3D object detector. At test time, objects are detected from a single view using our trained 3D detector. We further provide category labels for the vegetable present in single object scenes to facilitate association of labels to object 3D bounding boxes. More elaborate multiple instance learning techniques could be used to handle the general case of weakly annotated multi-object scenes [Mao et al. \(2019\)](#). We leave this for future work. We show extensive qualitative results in the veggie arrangement dataset as a proof that our model can effectively generalize to real world data if allowed multiview embodied supervision and weak category object labels.

4.1. Language conditioned scene generation

We show language-conditioned generated scenes for our model and the baseline model of Deng et al. [Deng et al. \(2018\)](#) in Figure 4 for utterances longer than those encountered at training time. The model of Deng et al. [Deng et al. \(2018\)](#) that generates a 2D RGB image directly (without an intermediate 3D representation) conditioned on a language utterance and its dependency tree. It predicts absolute 2D locations and 2D box sizes for objects and their 2D appearance feature maps, warped in predicted locations, and neurally decoded into an RGB image. We visualize our model’s predictions in two ways: i) **neural renders** are obtained by feeding the generated 3D assembled canvas to the 3D-to-2D neural projection module of GRNNs, ii) **Blender renders** are renderings of Blender scenes that contain object 3D meshes selected by small feature distance to the language generated object 3D feature tensors, and arranged based on the predicted 3D spatial offsets.

Our model re-samples an object location when they de-

tect the 3D intersection-over-union (IoU) computed from the predicted 3D object boxes of the newly added object with existing ones is higher than a cross-validated threshold of 0.1. The model of Deng et al. [Deng et al. \(2018\)](#) is trained to handle occluded objects. Notice though that it generates weird configurations as the number of objects increase. We tried imposing constraints of object placement using 2D IoU threshold in our baseline, but ran into the problem that we could not find plausible configurations for strict IoU thresholds, and we would obtain non-sensical configurations for low IoU thresholds, we include the results in the supplementary file. Note that 2D IoU cannot discriminate between physically plausible object occlusions and physically implausible object intersection. Reasoning about 3D object non intersection is indeed much easier in a 3D space.

More scene generation examples where predictions of our model are decoded from multiple camera viewpoints, more comparisons against the baseline and more details on Blender rendering visualization are included in Sections 2 and 3 of the supplementary file. Please note that **image generation is not the end-task for this work, rather, it is a task to help learn the mapping from language to the 3D space-aware abstract feature space.** We opt for a model that has reasoning capabilities over the generated entities, as opposed to generating pixel-accurate images that we cannot reason on.

4.2. Affordability inference of natural language utterances

We test our model and baselines in their ability to classify language utterances as describing sensible or non-sensical object configurations. We created a test set of 100 NL utterances, 50 of which are affordable, i.e., describe a realizable object arrangement, e.g., “*a red cube in front of a blue cylinder and in front of a red sphere, the blue cylinder is in front of the red sphere.*”, and 50 are unaffordable, i.e., describe a non-realistic object arrangement, e.g., “*a red cube is behind a cyan sphere and in front of a red cylinder, the cyan sphere is left behind the red cylinder.*”. In each utterance, an object is mentioned multiple times. The utterance is unaffordable when these mentions are contradictory. Answering correctly requires spatial reasoning over possible object configurations. **Both our model and baselines have been trained only on plausible utterances and scenes. We use our dataset only for evaluation.** This setup is similar to violation of expectation [Riochet et al. \(2019\)](#): the model detects violations while it has only been trained on plausible versions of the world.

Our model infers affordability of a language utterance by generating the 3D feature map of the described scene, as detailed in Section 3.2. When an object is mentioned multiple times in an utterance, our model uses the first mention to

mAP	ours RGB-D	Ren et al. (2015) RGB-D	ours RGB	Ren et al. (2015) RGB
2D	0.993	0.903	0.990	0.925
3D	0.973	-	0.969	-

Table 1: **Mean average precision for category agnostic region proposals.** Our 3D RPN outperforms the 2D state-of-the-art RPN of Faster R-CNN [Ren et al. \(2015\)](#).

add it in the 3D feature canvas, and uses that pairwise object spatial classifier D_S of Section 3.3 to infer if the predicted configuration also satisfies the later constraints. If not, our model re-samples object arrangements until a configuration is found or a maximum number of samples is reached.

We compare our model against a baseline based on the model of Deng et al. [Deng et al. \(2018\)](#). Similar to our model, when an object is mentioned multiple times, we use the first mention to add it in the 2D image canvas, and use pairwise object spatial classifiers we train over 2D bounding box spatial information—as opposed to 3D—to infer if the predicted configuration also satisfies the later constraints. Note that there are no previous works that attempt this language affordability inference task, and our baseline essentially performs similar operations as our model but in a 2D image generation space.

We consider a sentence to be affordable if the spatial classifier predicts a score above 0.5 for the later constraint. **Our model achieved an affordability classification accuracy of 95% while the baseline 79.3%.** The result suggests an improved ability to reason about affordable and non affordable object configurations in 3D as opposed to 2D image space.

4.3. Detecting spatial referential expressions

We use the same dataset and train/test split of scenes as in the previous section. For each annotated scene, we consider the first mentioned object as the one being referred to, that needs to be detected. In this task, we compare our model with a variant of the modular 2D referential object detector of Hu et al. [Hu et al. \(2016\)](#) that also takes as input the dependency parse tree of the expression. We train the object appearance detector for the baseline same as for our model using positive and negative examples but the inner product is on 2D feature space as opposed to 3D. We also train a pairwise spatial expression classifier to map width, height and x,y coordinates of the two 2D bounding boxes and the one-hot encoding of the spatial expression, e.g., “*in front of*” to a score reflecting whether the two boxes respect the corresponding arrangement. Note that our pairwise spatial expression classifier use 3D box information instead which helps it to generalize across camera placements.

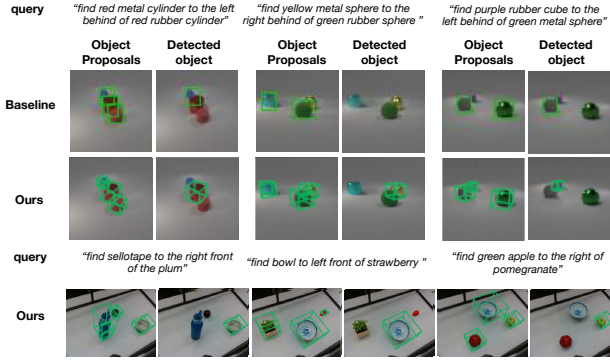


Figure 5: **Detecting referential spatial expressions.** Given a scene and a referential expression, our model localizes the object being referred to in 3D, while our baseline in 2D.

Our referential detectors are upper bounded by the performance of the Region Proposal Networks (RPNs) in 3D for our model and in 2D for the baseline, since we compare language-generated object feature tensors to object features extracted from 2D and 3D bounding box proposals. We compare RPN performance in Table 1. An object is successfully detected when the predicted box has an intersection over union (IoU) at least 0.5 with the groundtruth bounding box. For our model, we project the detected 3D boxes to 2D and compute 2D mean average precision (mean AP). Both our model and the baseline use a single RGB image as input as well as a corresponding depth map, which our model uses during the 2D-to-3D unprojection operation and the 2D RPN concatenates with the RGB input image. Our 3D RPN that takes the GRNN map \mathbf{M} as input better delineates the objects under heavy occlusions than the 2D RPN of faster-RCNN Ren et al. (2015).

We show quantitative results for referential expression detection in Table 2 with groundtruth as well as RPN predicted boxes, and qualitative results in Figure 5. In the “*in-domain view*” scenario, we test on camera viewpoints that have been seen at training time, in the “*out-domain view*” scenario, we test on **novel camera viewpoints**. An object is detected successfully when the corresponding detected bounding box has an IoU of 0.5 with the groundtruth box (in 3D for our model and in 2D for the baseline). Our model greatly outperforms the baseline for two reasons: a) it better detects objects in the scene despite heavy occlusions, and, b) even with groundtruth boxes, because the 3D representations of our model do not suffer from projection artifacts, they better generalize across camera viewpoints and object arrangements.

4.4. Manipulation instruction following

We use the PyBullet Physics simulator Coumans (2015) with similar setup as our CLEVR scenes. We use a simu-

	Ours	Hu et al. (2016)	Ours - GT 3D boxes	Hu et al. (2016) - GT 2D boxes
<i>in-domain view</i>	0.87	0.70	0.91	0.79
<i>out-domain view</i>	0.79	0.25	0.88	0.64

Table 2: **F1-Score for detecting referential expressions.** Our model greatly outperforms the baseline with both groundtruth and predicted region proposals, especially for novel camera views.

lated KUKA robot arm as our robotic platform. We use a *cube* and a *bowl*, using the same starting configuration for each scene, where the cube is held by the robot right above the bowl. We fix the end-effector to always point downwards, and we assume the object to be in robot’s hand at the beginning of each episode.

We compare our model against the 2D generative baseline of Deng et al. (2018) that generates object locations in 2D, and thus supply costs of the form: $\mathcal{C}^{2D}(\mathbf{x}_t) = \|\mathbf{x}_t^{2D} - \mathbf{x}_{goal}^{2D}\|_2^2$. We show in Table 3 success rates for different spatial expressions, where we define success as placing the object in the set of locations implied by the instruction. Goal locations provided in 2D do much worse in guiding policy search than target object locations in 3D supplied by our model. This is because 2D distances suffer from foreshortening and reflect planning distance worse than 3D ones. This is not surprising: in fact, the robotics control literature almost always considers desired locations of objects to be achieved to be in 3D Kumar et al. (2016); Levine et al. (2016). In our work, we link language instructions with such 3D inference using inverse graphics computer vision architectures for 2D to 3D lifting in an implicit learnable 3D feature space. Videos of the learnt language-conditioned placement policies can be found here : <https://sites.google.com/view/embodylanguagegrounding/home>

Language Exp.	left	left-behind	left-front	right	right-behind	right-front	inside
Baseline	4/5	1/5	3/5	0/5	2/5	0/5	1/5
Ours	5/5	3/5	5/5	5/5	5/5	3/5	5/5

Table 3: **Success rates for executing instructions regarding object placement.** Policies learnt using costs over 3D configurations much outperform those learnt with costs over 2D configurations.

5. Discussion - Future Work

We proposed models that learn to think visually about language meaning, by associating language utterances with compositional 3D feature representations of the objects and scenes the utterances describe, and exploiting the rich constraints of the 3D space for spatial reasoning. We showed our model can effectively imagine object spatial configurations conditioned on language utterances, can reason about affordability of spatial arrangements, detect objects in them, and train policies for following object placement instructions. We further showed our models generalize to real world data without real world examples of scenes annotated with spatial descriptions, rather, only single category labels. The language utterances we use are programmatically generated Johnson et al. (2016). One way to extend our framework to handle truly natural language is via paraphrasing such programmatically generated utterances Berant and Liang (2014) to create paired examples of natural language utterances and parse trees, then train a dependency parser Weiss et al. (2015) to generate dependency parse trees as input for our model using natural language as input. Going beyond basic spatial arrangements would require learning dynamics, physics and mechanics of the grounding 3D feature space. This, as well as handling natural language, are clear avenues for future work.

6. Acknowledgements

We would like to thank Shreshta Shetty and Gaurav Pathak for helping set up the table dome; Xian Zhou for help with the real robot placement experiments.

References

- Jacob Andreas, Marcus Rohrbach, Trevor Darrell, and Dan Klein. Learning to compose neural networks for question answering. In *North American Chapter of the Association for Computational Linguistics: Human Language Technologies (NAACL)*, 2016). 3
- Stanislaw Antol, Aishwarya Agrawal, Jiasen Lu, Margaret Mitchell, Dhruv Batra, C Lawrence Zitnick, and Devi Parikh. Vqa: Visual question answering. In *Proceedings of the IEEE International Conference on Computer Vision*, pages 2425–2433, 2015). 3
- Lisa Aziz-Zadeh, Christian Fiebach, Srinu Narayanan, Jerome Feldman, Ellen Dodge, and Richard Ivry. Modulation of the ffa and ppa by language related to faces and places. *Social neuroscience*, 3:229–38, 02 2008). 12
- Jonathan Berant and Percy Liang. Semantic parsing via paraphrasing. In *ACL (1)*, pages 1415–1425. The Association for Computer Linguistics, 2014). 9
- Benjamin Bergen. Mental simulation in spatial language processing. 01 2005). 12
- B Bergen. Experimental methods for simulation semantics. *Methods in cognitive linguistics*, pages 277–301, 2007). 12
- Benjamin Bergen. Embodiment, simulation and meaning. *The Routledge Handbook of Semantics*, pages 142–157, 01 2015). 12
- Volkan Cirik, Taylor Berg-Kirkpatrick, and Louis-Philippe Morency. Using syntax to ground referring expressions in natural images. In *AAAI*, 2018). 5
- Erwin Coumans. Bullet physics simulation. In *ACM SIGGRAPH 2015 Courses*, SIGGRAPH ’15, New York, NY, USA, 2015). ACM. 8
- Zhiwei Deng, Jiacheng Chen, YIFANG FU, and Greg Mori. Probabilistic neural programmed networks for scene generation. In S. Bengio, H. Wallach, H. Larochelle, K. Grauman, N. Cesa-Bianchi, and R. Garnett, editors, *Advances in Neural Information Processing Systems 31*, pages 4028–4038. Curran Associates, Inc., 2018). 3, 6, 7, 8, 11, 12, 13, 21
- Jacob Devlin, Hao Cheng, Hao Fang, Saurabh Gupta, Li Deng, Xiaodong He, Geoffrey Zweig, and Margaret Mitchell. Language models for image captioning: The quirks and what works. *arXiv preprint arXiv:1505.01809*, 2015). 3
- Bhuwan Dhingra, Hanxiao Liu, William W. Cohen, and Ruslan Salakhutdinov. Gated-attention readers for text comprehension. *CoRR*, abs/1606.01549, 2016). 1
- Jeff Donahue, Lisa Anne Hendricks, Sergio Guadarrama, Marcus Rohrbach, Subhashini Venugopalan, Kate Saenko, and Trevor Darrell. Long-term recurrent convolutional networks for visual recognition and description. In *IEEE Conference on Computer Vision and Pattern Recognition (CVPR)*, 2015). 3
- Hao Fang, Saurabh Gupta, Forrest Iandola, Rupesh K Srivastava, Li Deng, Piotr Dollár, Jianfeng Gao, Xiaodong He, Margaret Mitchell, John C Platt, et al. From captions to visual concepts and back. In *Proceedings of the IEEE conference on computer vision and pattern recognition*, pages 1473–1482, 2015). 3
- Jerome Feldman and Srinivas Narayanan. Embodied meaning in a neural theory of language. *Brain and language*, 89:385–92, 06 2004). 12
- Jerome A. Feldman. *From Molecule to Metaphor: A Neural Theory of Language*. MIT Press, Cambridge, MA, 2006). 12
- James J. Gibson. *The Ecological Approach to Visual Perception*. Houghton Mifflin, 1979). 12
- Arthur Glenberg and Michael P. Kaschak. Grounding language in action. *Psychonomic Bulletin and Review*, 9(3):558–565, 9 2002). 12
- A. Glenberg and D. Robertson. Symbol grounding and meaning: A comparison of high-dimensional and embodied theories of meaning. *Journal of Memory and Language*, 2000). 12
- Kaiming He, Georgia Gkioxari, Piotr Dollár, and Ross B. Girshick. Mask R-CNN. *CoRR*, abs/1703.06870, 2017). 4
- Karl Moritz Hermann, Tomas Kocisky, Edward Grefenstette, Lasse Espeholt, Will Kay, Mustafa Suleyman, and Phil Blunsom. Teaching machines to read and comprehend. In C. Cortes, N. D. Lawrence, D. D. Lee, M. Sugiyama, and R. Garnett, editors, *Advances in Neural Information Processing Systems 28*, pages 1693–1701. Curran Associates, Inc., 2015). 1
- Ronghang Hu, Marcus Rohrbach, Jacob Andreas, Trevor Darrell, and Kate Saenko. Modeling relationships in referential expressions with compositional modular networks. 11 2016). 3, 5, 7, 8
- Justin Johnson, Bharath Hariharan, Laurens van der Maaten, Li Fei-Fei, C. Lawrence Zitnick, and Ross B. Girshick. CLEVR: A diagnostic dataset for compositional language and elementary

- visual reasoning. *CoRR*, abs/1612.06890, 2016). 3, 6, 9
- Rudolf Kadlec, Martin Schmid, Ondrej Bajgar, and Jan Kleindienst. Text understanding with the attention sum reader network. *CoRR*, abs/1603.01547, 2016). 1
- Andrej Karpathy and Li Fei-Fei. Deep visual-semantic alignments for generating image descriptions. In *Proceedings of the IEEE Conference on Computer Vision and Pattern Recognition*, pages 3128–3137, 2015). 3
- Tejas D. Kulkarni, Will Whitney, Pushmeet Kohli, and Joshua B. Tenenbaum. Deep convolutional inverse graphics network. *CoRR*, abs/1503.03167, 2015). 2
- Vikash Kumar, Abhishek Gupta, Emanuel Todorov, and Sergey Levine. Learning dexterous manipulation policies from experience and imitation. *CoRR*, abs/1611.05095, 2016). 8
- Sergey Levine, Chelsea Finn, Trevor Darrell, and Pieter Abbeel. End-to-end training of deep visuomotor policies. *J. Mach. Learn. Res.*, 17(1):1334–1373, Jan. 2016). 8
- Roel M Willems, Ivan Toni, Peter Hagoort, and Daniel Casasanto. Neural dissociations between action verb understanding and motor imagery. *Journal of cognitive neuroscience*, 22:2387–400, 11 2009). 12
- Jiayuan Mao, Chuang Gan, Pushmeet Kohli, Joshua B. Tenenbaum, and Jiajun Wu. The Neuro-Symbolic Concept Learner: Interpreting Scenes, Words, and Sentences From Natural Supervision. In *International Conference on Learning Representations*, 2019). 6
- Bruno A. Olshausen. Perception as an inference problem. 2013). 1
- Shaoqing Ren, Kaiming He, Ross Girshick, and Jian Sun. Faster r-cnn: Towards real-time object detection with region proposal networks. In C. Cortes, N. D. Lawrence, D. D. Lee, M. Sugiyama, and R. Garnett, editors, *Advances in Neural Information Processing Systems* 28, pages 91–99. Curran Associates, Inc., 2015). 7, 8
- Ronan Riochet, Mario Yncente Castro, Mathieu Bernard, Adam Lerer, Rob Fergus, Véronique Izard, and Emmanuel Dupoux. Intphys: A benchmark for visual intuitive physics reasoning. 2019). 7
- Anna Rohrbach, Marcus Rohrbach, Niket Tandon, and Bernt Schiele. A dataset for movie description. In *IEEE Conference on Computer Vision and Pattern Recognition (CVPR)*, 2015). 3
- Anna Rohrbach, Marcus Rohrbach, Siyu Tang, Seong Joon Oh, and Bernt Schiele. Generating descriptions with grounded and co-referenced people. In *IEEE Conference on Computer Vision and Pattern Recognition (CVPR)*, 2017). 3
- Marcus Rohrbach, Sikandar Amin, Mykhaylo Andriluka, and Bernt Schiele. A database for fine grained activity detection of cooking activities. In *IEEE Conference on Computer Vision and Pattern Recognition (CVPR)*. IEEE, 2012). 3
- Marcus Rohrbach, Qiu Wei, Ivan Titov, Stefan Thater, Manfred Pinkal, and Bernt Schiele. Translating video content to natural language descriptions. In *IEEE International Conference on Computer Vision (ICCV)*, 2013). 3
- Lukasz Romaszko, Christopher K. I. Williams, Pol Moreno, and Pushmeet Kohli. Vision-as-inverse-graphics: Obtaining a rich 3d explanation of a scene from a single image. In *The IEEE International Conference on Computer Vision (ICCV) Workshops*, Oct 2017). 2
- Ayşe Pinar Saygin, Stephen Mccullough, Morana Alac, and Karen Emmorey. Modulation of bold response in motion-sensitive lateral temporal cortex by real and fictive motion sentences. *Journal of cognitive neuroscience*, 22:2480–90, 11 2009). 12
- Meet Shah, Xinlei Chen, Marcus Rohrbach, and Devi Parikh. Cycle-consistency for robust visual question answering. *CoRR*, abs/1902.05660, 2019). 3
- Noam Shazeer, Azalia Mirhoseini, Krzysztof Maziarczyk, Andy Davis, Quoc Le, Geoffrey Hinton, and Jeff Dean. Outrageously large neural networks: The sparsely-gated mixture-of-experts layer. 2017). 4
- Yuval Tassa, Nicolas Mansard, and Emanuel Todorov. Control-limited differential dynamic programming. *2014 IEEE International Conference on Robotics and Automation (ICRA)*, pages 1168–1175, 2014). 6
- Fish Tung and Katerina Fragkiadaki. Reward learning using natural language. *CVPR*, 2018). 5, 6
- Hsiao-Yu Fish Tung, Adam W. Harley, William Seto, and Katerina Fragkiadaki. Adversarial inverse graphics networks: Learning 2d-to-3d lifting and image-to-image translation from unpaired supervision. *CoRR*, abs/1705.11166, 2017). 2
- Hsiao-Yu Fish Tung, Ricson Cheng, and Katerina Fragkiadaki. Learning spatial common sense with geometry-aware recurrent networks. In *The IEEE Conference on Computer Vision and Pattern Recognition (CVPR)*, June 2019). 2, 3, 4
- Ramakrishna Vedantam, Xiao Lin, Tanmay Batra, C. Lawrence Zitnick, and Devi Parikh. Learning common sense through visual abstraction. In *International Conference on Computer Vision (ICCV)*, 2015). 3
- David Weiss, Chris Alberti, Michael Collins, and Slav Petrov. Structured training for neural network transition-based parsing. *CoRR*, abs/1506.06158, 2015). 9
- Jason Weston, Sumit Chopra, and Antoine Bordes. Memory networks. *CoRR*, abs/1410.3916, 2014). 1
- Zichao Yang, Xiaodong He, Jianfeng Gao, Li Deng, and Alexander J. Smola. Stacked attention networks for image question answering. *CoRR*, abs/1511.02274, 2015). 3

7. Model details: Language-conditioned 3D visual imagination

We train our stochastic generative networks using conditional variational autoencoders. For the *what* generative module, our inference network conditions on the word embeddings of the adjectives and the noun in the noun phrase, as well as the 3D feature tensor obtained by cropping the 3D feature map $\mathbf{M} = \text{GRNN}(I)$ using the ground-truth 3D bounding box of the object the noun phrase concerns. For the *where* generative module, the corresponding inference network conditions on one-hot encoding of the spatial expression, as well as the 3D relative spatial offset, available from 3D object box annotations. Inference networks are used only at training time. Our *what* and *where* decoders take the posterior noise and predict 3D object appearance feature tensors, and cross-object 3D spatial offsets, respectively, for each object. We add predicted object feature tensors at predicted 3D locations in a 3D feature canvas. Our reconstruction losses ask the language-generated and image-inferred 3D feature maps from GRNNs to be close in feature distance, both in 3D and after 2D neural projection using the GRNN 3D-to-2D neural decoder, and the predicted cross-object 3D relative spatial offsets to be close to the ground-truth cross-object 3D relative offsets.

8. Experimental details: Language conditioned scene generation

We visualize our model’s predictions in two ways: i) **neurally rendered** are obtained by feeding the generated 3D assembled canvas to the 3D-to-2D neural projection module of GRNNs, ii) **Blender rendered** are renderings of Blender scenes that contain object 3D meshes selected by small feature distance to the language generated object 3D feature tensors, and arranged based on the predicted 3D spatial offsets.

We consider a database of 300 object 3D meshes to choose from. To get the object feature tensor for a candidate 3D object model, we render multi-view RGB-D data of this object in Blender, and input them to the GRNN to obtain the corresponding feature map, which we crop using the groundtruth bounding box. Blender renders better convey object appearance because the neurally rendered images are blurry. Despite pixel images being blurry, our model retrieves correct object meshes that match the language descriptions.

9. Additional experiments

Scene generation conditioned on natural language In Figure 6, we compare our model with the model of Deng et al. (Deng et al. (2018)) on language to scene generation with utterances longer than those used during training time. We

show both neural and Blender rendering of scenes predicted from our model. We remind the reader that a Blender rendering is computed by using the cross-object relative 3D offsets predicted by our model, and using the generated object 3D feature tensors to retrieve the closest matching meshes from a training set. Our training set is comprised of 100 objects with known 3D bounding boxes, and for each we compute a 3D feature tensor by using the 2D-to-3D unprojection module described above, and cropping the corresponding sub-tensor based on the 3D bounding box coordinates of the object. Despite our neural rendering being blurry, we show the features of our generative networks achieve correct nearest neighbor retrieval. The generation results show our model can generalize to utterances that are much longer than those in the training data. In Figure 7, we show rendering results from our model on our real world dataset.

One key feature of our model is that it generates a scene as opposed to an independent static image. In Figure 8, we show rendering images from the 3D feature tensor across different viewpoints. The rendering images are consistent across viewpoints. For a 2D baseline Deng et al. (2018), it is unclear how we can obtain a set of images that not only match with input sentence but also are consistent with each others.

We show in Figures 9-10 more neural and Blender rendering of scenes predicted from our model, conditioning on parse trees of natural language utterances. In 11, we show rendering results learned from our real world dataset.

Scene generation conditional on natural language and visual context In Figures 12-14 we show examples of scene generation from our model when conditioned on both natural language and the visual context of the agent. In this case, some objects mentioned in the natural language utterance are present in the agent’s environment, and some are not. Our model uses a 3D object detector to localize objects in the scene, and the learnt 2D-to-3D unprojection neural module to compute a 3D feature tensor for each, by cropping the scene tensor around each object. Then, it compares the object tensors generated from natural language to those generated from the image, and if a feature distance is below a threshold, it grounds the object reference in the parse tree of the utterance to object present in the environment of the agent. If such binding occurs, as is the case for the “green cube” in the top left example, then our model uses the image-generated tensors of the binded objects, instead of the natural language generated ones, to complete the imagination. In this way, our model grounds natural language to both perception and imagination.

Affordability inference based on 3D non-intersection Objects do not intersect in 3D. Our model has a 3D fea-

ture generation space and can detect when this basic principle is violated. The baseline model of [Deng et al. \(2018\)](#) directly generates 2D images described in the utterances (conditioned on their parse tree) without an intermediate 3D feature space. Thus, it performs such affordability checks in 2D. However, in 2D, objects frequently occlude one another, while they still correspond to an affordable scene. In Figure 15, we show intersection over union scores computed in 3D by our model and in 2D by the baseline. While for our model such scores correlate with affordability of the scene (e.g., the scenes in 1st, third, and forth columns in the first row are clearly non-affordable as objects interpenetrate) the same score from the baseline is not an indicator of affordability, e.g., the last column in the last row of the figure can in fact be a perfectly valid scene, despite the large IoU score.

Language-guided placement policy learning In Figure 16, we show the initial and final configurations of the learned policy using different referential expression. The robot can successfully place the object to the target location given the referential expression. We also show in the supplementary a video of a real robot executing the task.

10. Additional related work

The inspiring experiments of Glenberg and Robertson [Glenberg and Robertson \(2000\)](#) in 1989 demonstrated that humans can easily judge the plausibility—they called it *affordability*—of natural language utterances, such as “*he used a newspaper to protect his face from the wind*”, and the implausibility of others, such as “*he used a matchbox to protect his face from the wind*”. They suggest that humans associate words with actual objects in the environment or prototypes in their imagination that retain perceptual properties—how the objects look—and affordance information [Gibson \(1979\)](#)—how the objects can be used. A natural language utterance is then understood through perceptual and motor *simulations* of explicitly and implicitly mentioned nouns and verbs, in some level of abstraction, that encode such affordances. For example, the matchbox is too small to protect a human face from the wind, while a newspaper is both liftable by a human and can effectively cover a face when held appropriately. This hypothesis is currently better known as simulation semantics [Feldman and Narayanan \(2004\)](#); [Feldman \(2006\)](#); [Bergen \(2005, 2015\)](#) and has extensive empirical support: reaction times for visual or motor operations are shorter when human subjects are shown a related sentence [Glenberg and Kaschak \(2002\)](#); [Bergen \(2007\)](#), and MRI activity is increased in the brain’s vision system or motor areas when human subjects are shown vision- or motor-related linguistic concepts, respectively [Aziz-Zadeh et al. \(2008\)](#); [M Willems et al. \(2009\)](#); [Saygin et al. \(2009\)](#). This paper proposes

an initial computational model for the simulation semantics hypothesis for the language domain of object spatial arrangements.

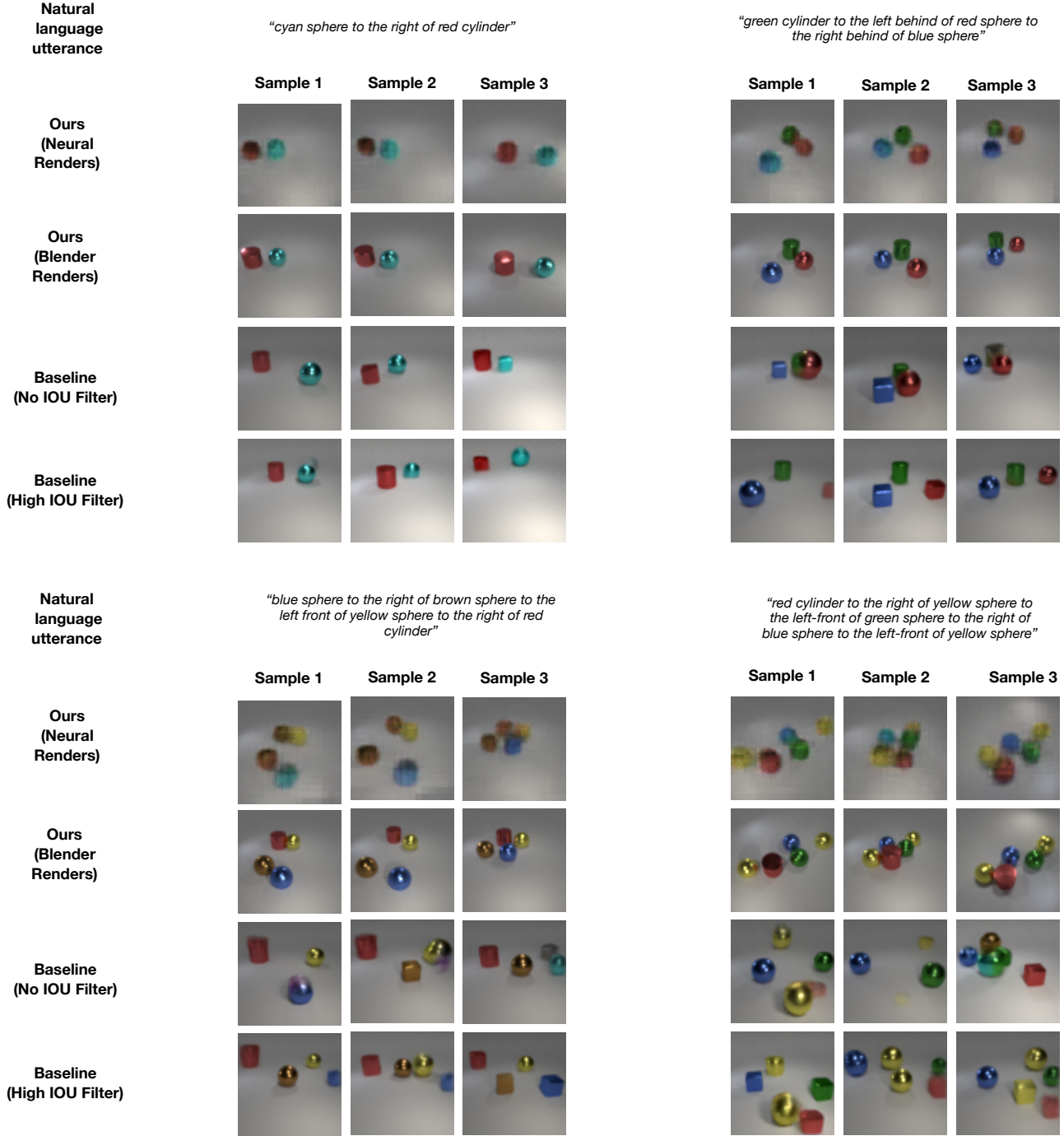


Figure 6: **Language to scene generation** from our model (Row1, Row2) and the model of Deng et al [Deng et al. \(2018\)](#) (Row 3, 4) for utterances longer than those encountered at training time. Both our model and the baseline are stochastic, and we sample three generated scenes/images per utterance. (Row 1 and Row 2) shows neural and Blender rendering results from our model. For the Blender rendering, we retrieve the closet 3D object mesh using the features of our generative networks, and place the retrieved objects in the corresponding locations in Blender to render an image. (Row 3) shows image generation results with no IoU constraint during sampling for the baseline. This means objects might go out of the field of view. (Row 4) shows result with high IoU constraint.

**Natural
language
utterance**

*"tomato to the front of avocado to the left of
yellow lemon to the behind of pomegranate"*

*"banana to the behind of red apple to the left
of green grapes"*

**Ours
(Neural
Renders)**



**Natural
language
utterance**

*"yellow lemon to the behind of pomegranate to
the left front of pear to the front of toy truck"*

*"orange to the front of banana to the left behind
of red apple"*

**Ours
(Neural
Renders)**



Figure 7: **Language to image generation** on our real world data. We sample three different scenes for each natural language utterances.

**Natural
language
utterance**

*"red cylinder to the right of yellow sphere to the left-front of green sphere to the right of blue sphere to
the left-front of yellow sphere"*

Ref. (0°)

60°

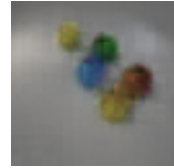
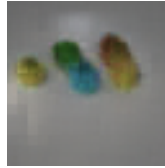
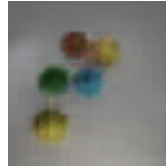
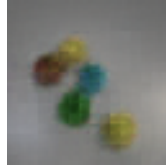
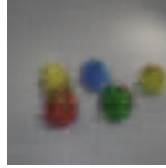
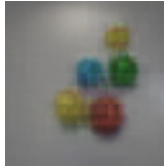
120°

180°

240°

300°

**Ours
(Neural
Renders)**



**Ours
(Blender
Renders)**

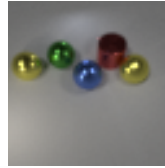
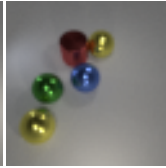
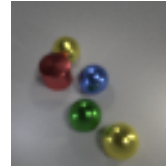
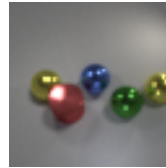


Figure 8: **Consistent scene generation** . We render the generated 3D feature canvas from various viewpoints in the first row using the neural GRNN decoder, and compare against the different viewpoint projected Blender rendered scenes. Indeed, our model correctly predicts occlusions and visibilities of objects from various viewpoints, and can generalize across different number of objects. 2D baselines do not have such imagination capability.

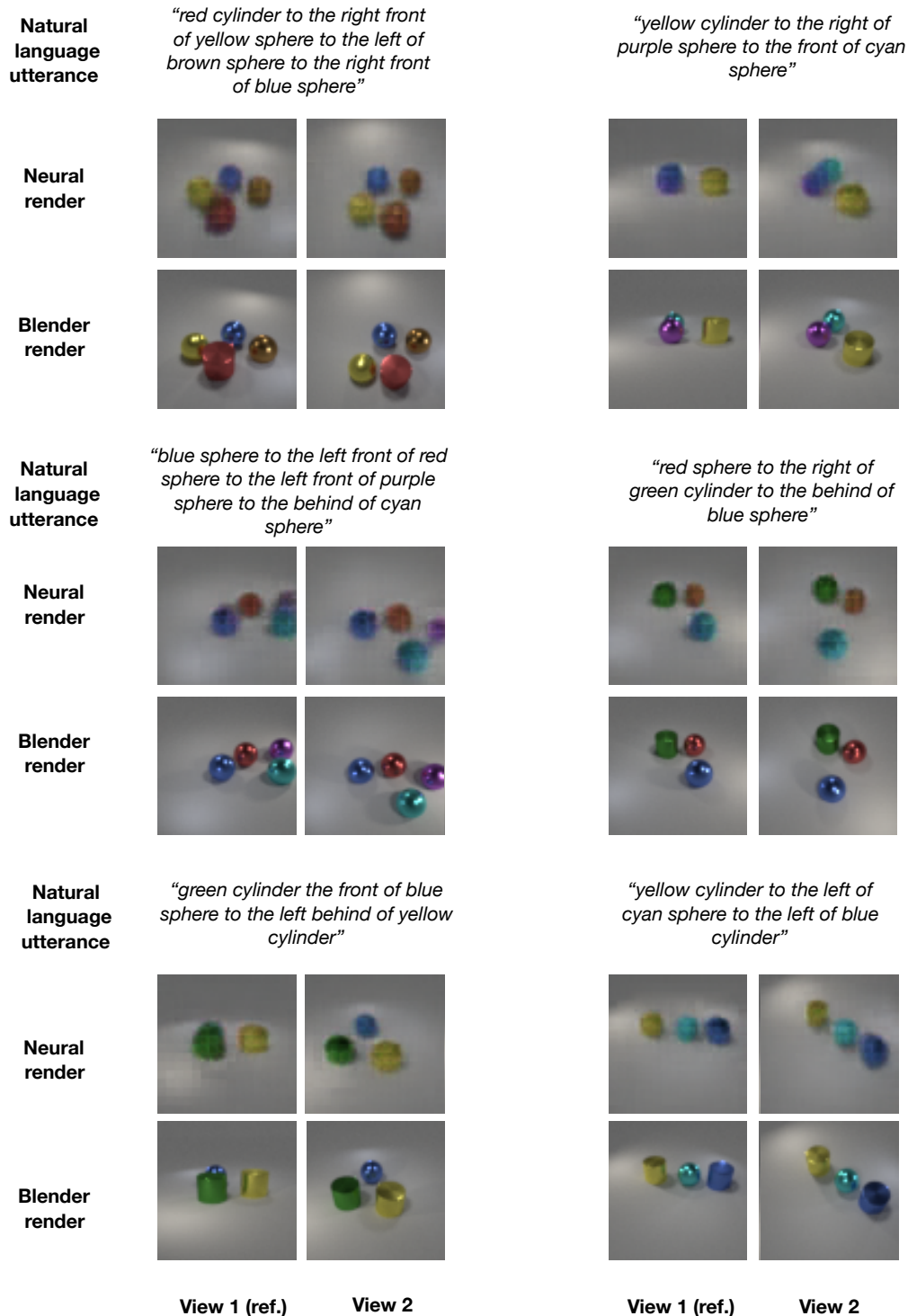


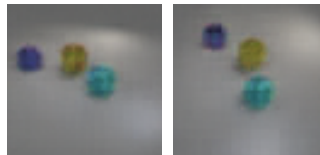
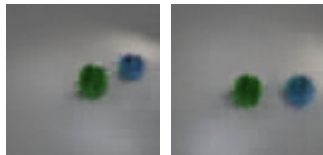
Figure 9: **Natural language conditioned neural and blender scene renderings generated by the proposed model.** We visualize each scene from two nearby views, a unique ability of our model, due to its 3-dimensional generation space.

**Natural
language
utterance**

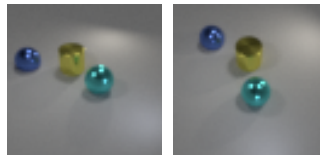
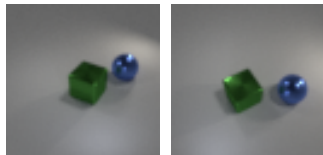
*“green cube to the left front of
blue sphere”*

*“cyan sphere to the right front of
yellow cylinder to the right of blue
sphere”*

**Neural
render**



**Blender
render**

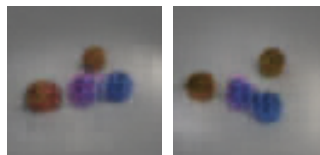
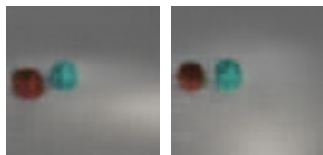


**Natural
language
utterance**

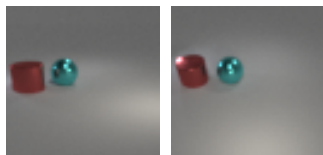
*“red cylinder to the left front of
cyan sphere”*

*“brown sphere to the behind of
purple sphere to the left of blue
sphere to the right of brown
sphere ”*

**Neural
render**



**Blender
render**

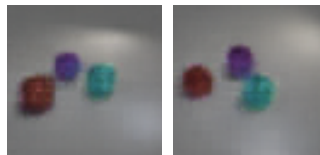
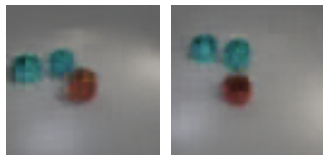


**Natural
language
utterance**

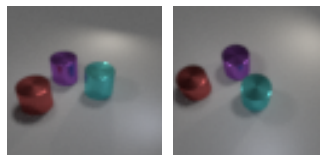
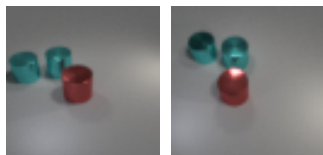
*“cyan cylinder to the left of cyan
cylinder to the left behind of red
cylinder”*

*“red cylinder to the left front
of purple cylinder to the left
behind of cyan cylinder”*

**Neural
render**



**Blender
render**



View 1 (ref.)

View 2

View 1 (ref.)

View 2

Figure 10: (Additional) Natural language conditioned neural and blender scene renderings generated by the proposed model.

**Natural
language
utterance**

"cup to the left of helmet"

**Neural
render**



*"yellow lemon to the behind of saturn
peach to the right of yellow lemon to
the front of saturn peach"*



**Natural
language
utterance**

*"red apple to the left of orange to
the front of cup to the right of
pomegranate"*

**Neural
render**



*"toy truck to the left of yellow lemon to
the front of pomegranate to the right of
pear"*



**Natural
language
utterance**

*"orange to the left of headphone to
the front of pomegranate to the
right of plum to the left behind of
yellow lemon to the behind of
yellow lemon "*

**Neural
render**



*"red apple to the front of yellow lemon to the left
behind of saturn peach to the front of plum to
the left behind of water bottle to the front of
pomegranate the left behind of yellow lemon to
the behind of yellow lemon"*



**Natural
language
utterance**

*"red apple to right behind of green
grapes"*

**Neural
render**



*"red apple to the front of orange to the
left behind of saturn peach to the front
of plum to the left behind of
pomegranate to the behind of
headphone to the left front of yellow
lemon to the behind of yellow lemon"*



**Natural
language
utterance**

*"toy dinosaur to the left front of
orange "*

**Neural
render**



*"ball to the left front of red apple to the
left of tomato to the behind of saturn
peach"*



View 1 (ref.)

View 2

View 1 (ref.)

View 2

Figure 11: (Additional) Natural language conditioned neural scene renderings generated by the proposed model over our real world dataset.

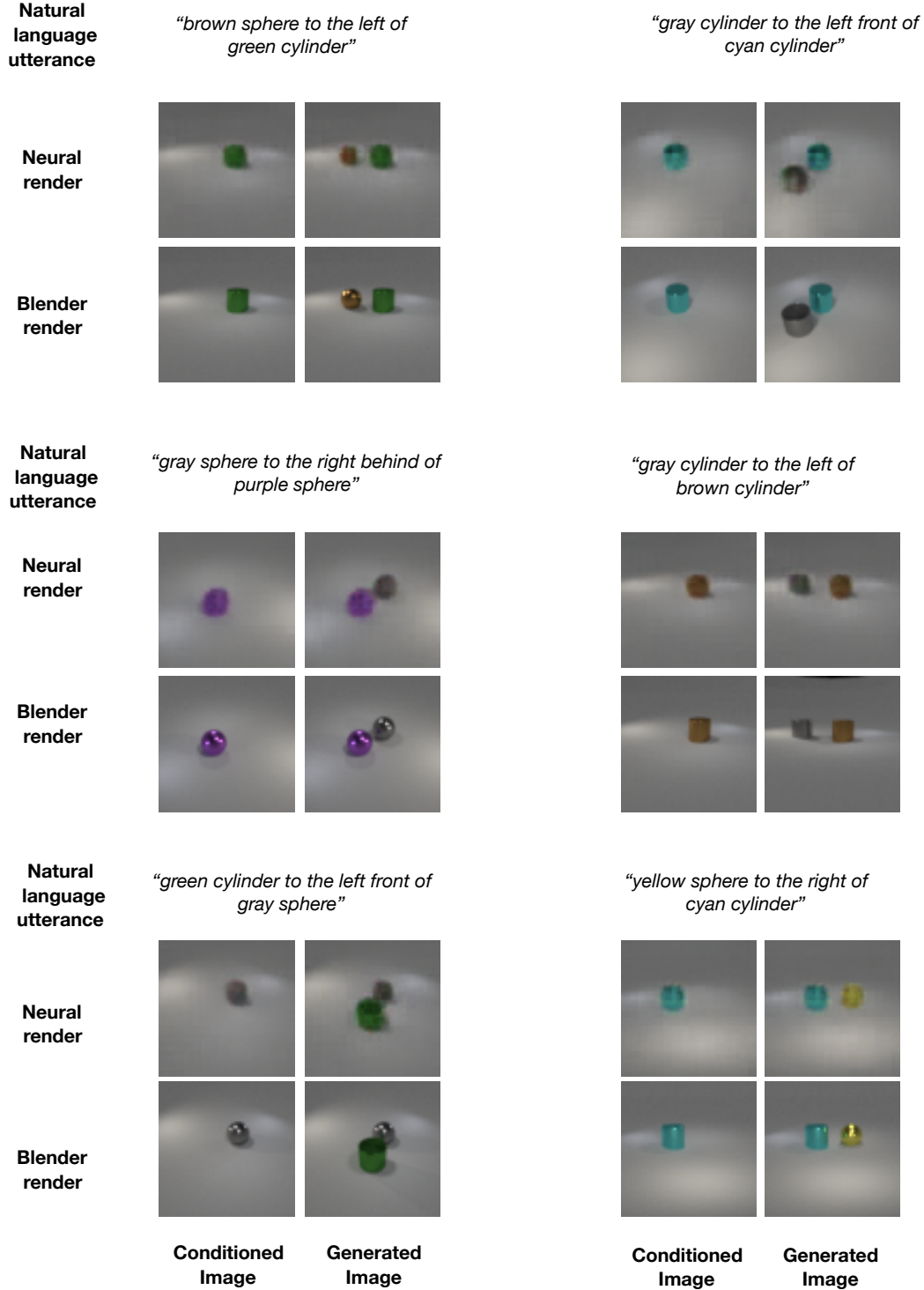


Figure 12: **Neural and blender scene renderings generated by the proposed model, conditioned on natural language and the visual scene.** Our model uses a 3D object detector to localize objects in the scene, and the learnt 2D-to-3D unprojection neural module to compute a 3D feature tensor for each, by cropping accordingly the scene tensor. Then, it compares the natural language conditioned generated object tensors to those obtained from the image, and grounds objects references in the parse tree of the utterance to objects presents in the environment of the agent, if the feature distance is below a threshold. If such binding occurs, as is the case for the “green cube” in top left, then, our model used the image-generated tensors of the binded objects, instead of the natural language generated ones, to complete the imagination. In this way, our model grounds natural language to both perception and imagination.

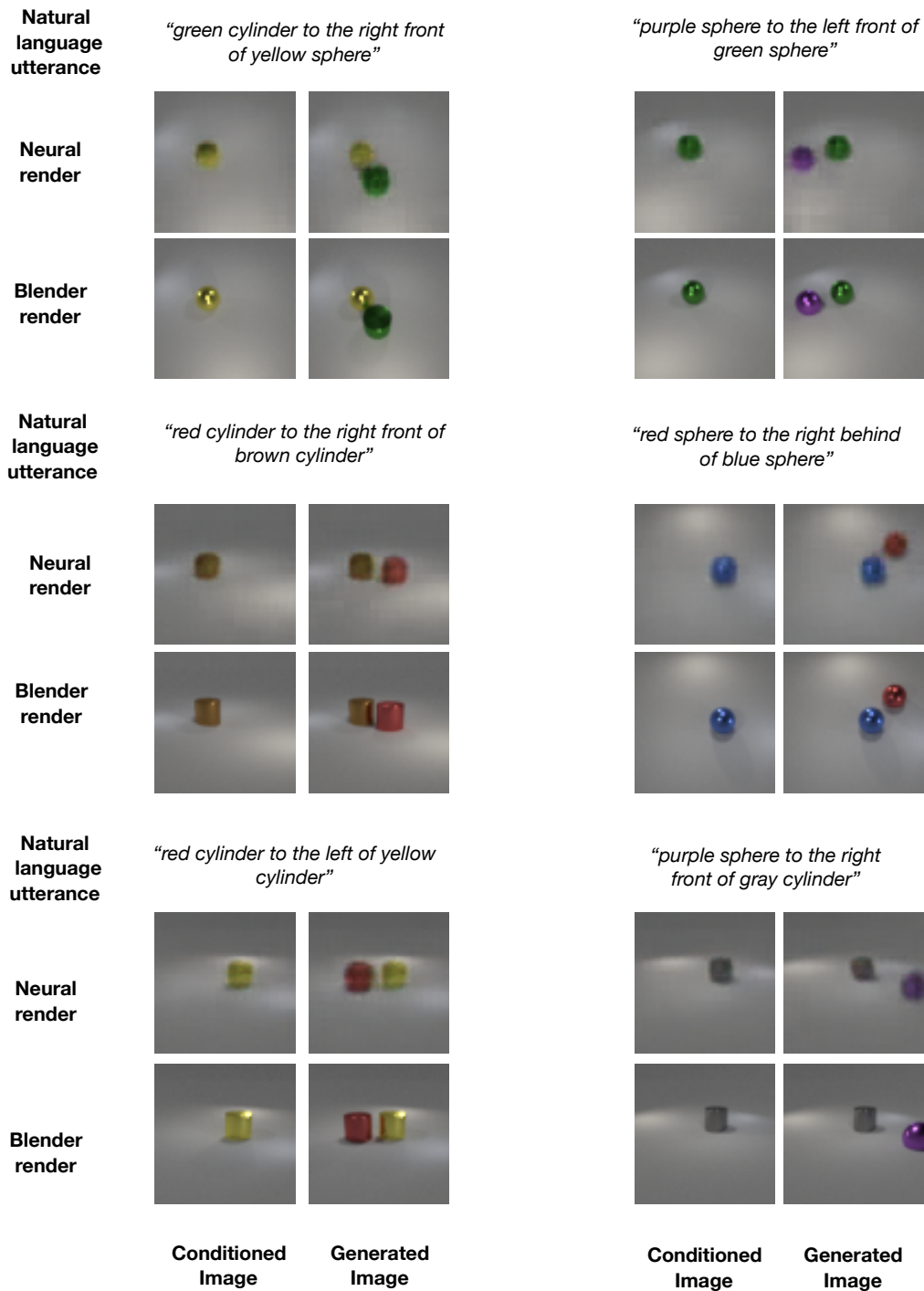


Figure 13: (Additional) Neural and blender scene renderings generated by the proposed model, conditioned on natural language *and* the visual scene.

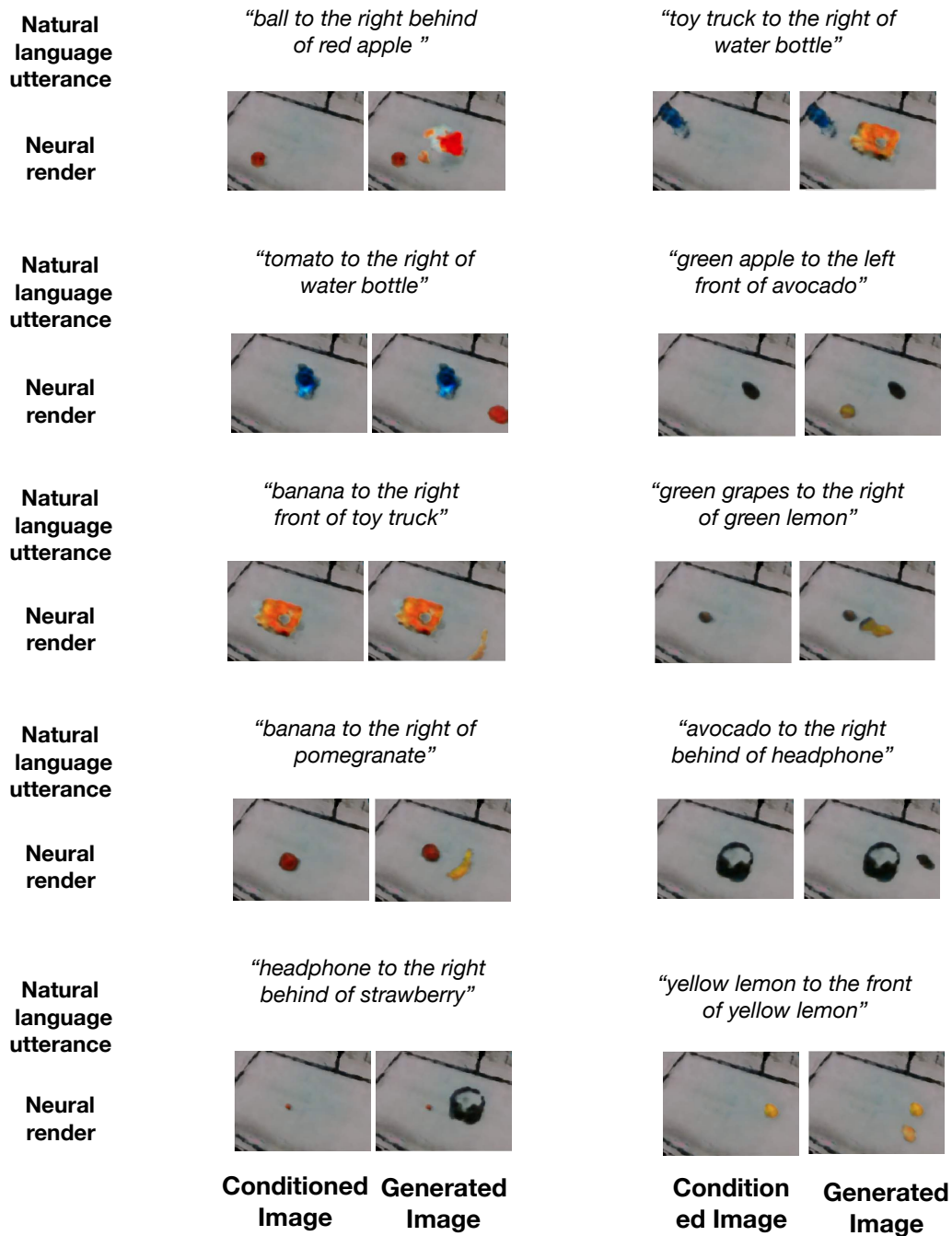


Figure 14: (Additional) Neural scene renderings generated by the proposed model, conditioned on natural language *and* the visual scene from our real world dataset.

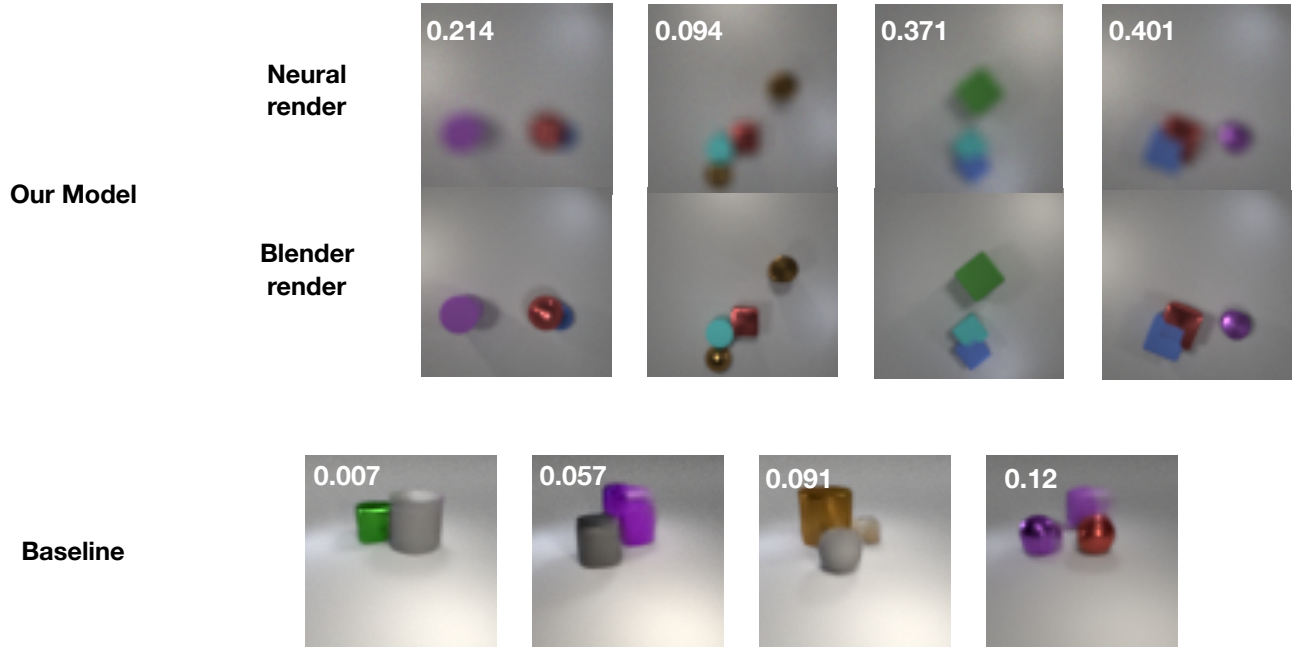


Figure 15: **Affordability prediction comparison of our model with the baseline work of Deng et al. (2018).** In the top 2 rows, we show the Neural and Blender renderings of our model. Since we reason about the scene in 3D, our model allows checks for expression affordability by computing the 3D intersection-over-union (IoU) scores. In contrast, the bottom row shows the baseline model which operates in 2D latent space and hence cannot differentiate between 2D occlusions and overlapping objects in 3D.

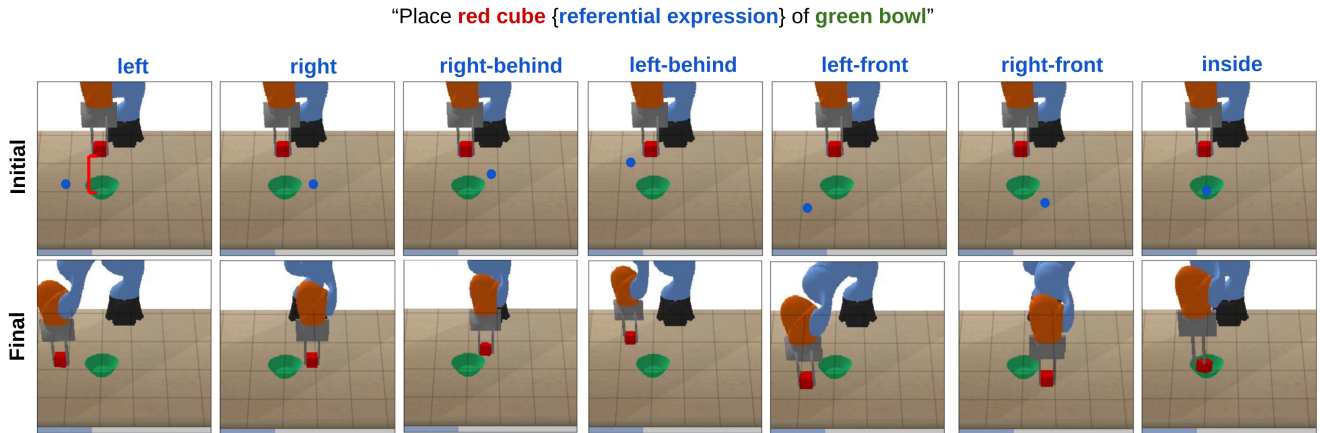


Figure 16: **Language-guided placement policy learning.** We show the final configurations of the learned policy using different referential expressions for the utterance "Place red cube {referential expression} of green bowl." *Top:* Initial robot configuration with the goal position generated by our method indicated as a blue dot. *Bottom:* Final robot configuration. We can see that the robot successfully places the cube with respect to the bowl according to the given referential expression.